Danilenko, Aleksandr; Rastgou, Masoud; Manoocheri, Farshid; Kinnunen, Jussi; Korpelainen, Virpi; Lassila, Antti; Ikonen, Erkki

Reflectometry technique for study of complex multilayer micro- and nanostructures with lateral periodicity

Published in:
Journal of Applied Physics

DOI:
10.1063/5.0246125

Published: 07/03/2025

Document Version
Publisher's PDF, also known as Version of record

Please cite the original version:
Danilenko, A., Rastgou, M., Manoocheri, F., Kinnunen, J., Korpelainen, V., Lassila, A., & Ikonen, E. (2025). Reflectometry technique for study of complex multilayer micro- and nanostructures with lateral periodicity. *Journal of Applied Physics*, *137*(9), Article 095302. https://doi.org/10.1063/5.0246125

Journal of Applied Physics

RESEARCH ARTICLE | MARCH 03 2025

Reflectometry technique for study of complex multilayer micro- and nanostructures with lateral periodicity

Aleksandr Danilenko ; Masoud Rastgou ; Farshid Manoocheri ; Jussi Kinnunen ; Virpi Korpelainen ; Antti Lassila ; Erkki Ikonen

J. Appl. Phys. 137, 095302 (2025)
https://doi.org/10.1063/5.0246125

AIP Publishing

Journal of Applied Physics | ARTICLE | pubs.aip.org/aip/jap

Reflectometry technique for study of complex multilayer micro- and nanostructures with lateral periodicity

Cite as: J. Appl. Phys. **137**, 095302 (2025); doi: 10.1063/5.0246125
Submitted: 30 October 2024 · Accepted: 4 February 2025 ·
Published Online: 3 March 2025

View Online Export Citation CrossMark

Aleksandr Danilenko,[1,a)] Masoud Rastgou,[1] Farshid Manoocheri,[1] Jussi Kinnunen,[2] Virpi Korpelainen,[3] Antti Lassila,[3] and Erkki Ikonen[1,3]

AFFILIATIONS

[1]Metrology Research Institute, Aalto University, Maarintie 8, Espoo 02150, Finland
[2]Chipmetrics Oy, Yliopistokatu 7, Joensuu 80130, Finland
[3]VTT MIKES, Tekniikantie 1, Espoo 02150, Finland

[a)]**Author to whom correspondence should be addressed:** aleksandr.danilenko@aalto.fi. **Telephone:** +358 50 472 4064.

ABSTRACT

This study introduces a reflectometry-based technique for characterizing complex thin-film structures with lateral periodicity, using only a single, large-beam measurement to capture essential structural information. The PillarHall test chip structure, selected as a case study, features an air gap of 500 nm nominal thickness inside a layer structure with periodically repeated lateral structure elements. Using a non-destructive reflectometry technique, the sample's layer structure was analyzed through spectral reflectance measurements, conducted with a Cary 7000 spectrometer, and processed with a dedicated MATLAB code that incorporates the transfer matrix method to model and fit the reflectance spectrum. Two models, a basic and an advanced four-layer model, were developed and tested by fitting the simulated reflectance spectrum to a measured one. While the basic model provides sufficient information about the thin-film structure, the advanced model considers detailed variations in the thickness across the sample caused by specific structural features. Reflectometry results on structural sizes agree with direct profilometry measurements, supporting the method's reliability. These findings demonstrate that a single, large-beam measurement can yield comprehensive insights, positioning reflectometry as a robust tool for the advanced thin-film characterization of complex periodic structures.

I. INTRODUCTION

The development of new technologies in electronics is accompanied by new techniques for characterizing micro- and nanoscale structures, which is essential nowadays as modern electronics push the limits of miniaturization, particularly with the advancement of three-dimensional (3D) semiconductor technologies.[1–3] Traditional methods for assessing multilayer thin-film properties, such as cross-sectional electron microscopy,[4–6] present significant limitations for industry-scale applications due to their time-consuming and invasive nature. Existing non-destructive methods, including x-ray computed tomography, Mueller-matrix ellipsometry, and ptychographic reflectometry, are also often time-consuming or complex.[7–9] These challenges drive the need for efficient, non-destructive techniques capable of characterizing complex structures, especially thin films used in advanced semiconductor devices.

To address this need, we introduce an advanced model within the framework of reflectometry,[9–13] developed to enhance the accuracy of structural characterization of thin-film samples with lateral periodic geometries. This technique eliminates the need for extensive mapping scans across the sample's surface, unlike traditional methods that rely on multiple measurements across various points. Instead, our approach requires only a single reflectance measurement of the sample's surface with a large-area beam, which, when analyzed, provides comprehensive information about the thin-film structure, including critical details about its periodic features. This significantly simplifies the characterization process, making it

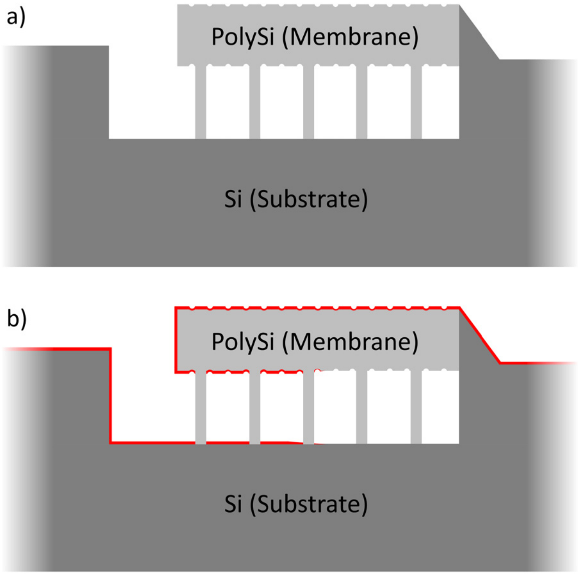

FIG. 1. (a) Schematic side view of the studied PillarHall test chip with uncoated structure for our reflectometry measurements. (b) Schematic side view of the PillarHall chip with the coated structure in the actual use of the component: penetration of the coating layer (shown as red) can be studied in high-aspect ratio structures after removing the membrane. The dimensions in Figs. 1, 4, and 7 are not drawn to the scale of real PillarHall samples.

potentially more time-efficient while retaining high accuracy in identifying structural variations and layer thicknesses.

Our model builds on the transfer matrix method (TMM),[14] incorporating detailed parameters that account for thickness variations across layered structures. This approach makes the model especially valuable for assessing samples with non-uniform thickness distributions or variations in optical properties. Nevertheless, it is worth noting that, while our approach effectively provides information about the size of structural features, it may lack the detailed spatial resolution offered by other techniques that perform point-to-point mapping scans of the sample.

We demonstrate the applicability of the developed method using the PillarHall test chip,[15–17] a reference sample for evaluating the conformality of thin films deposited by atomic layer deposition and chemical vapor deposition techniques. The PillarHall chip structure, with its air gap (AG) layer and periodically repeated structural elements, serves as an ideal test case for validating the model's capabilities. Because of PillarHall's structural complexity, specifically the presence of the air gap, these samples are fragile. This is where the reflectometry technique is perfectly suitable for the characterization task,[9–13] because it is a non-destructive method, which has previously proven effective for precise thin-film thickness characterization. By fitting reflectance data from the PillarHall sample, our model successfully retrieves the thicknesses of individual layers and size of structural features such as thickness variations in the polycrystalline silicon (PolySi) layer and air gap. Comparison of the results with optical profilometry illustrates model's potential to offer comprehensive insights into complex layered structures, opening opportunities for broader application of reflectometry techniques in the semiconductor industry.

II. STRUCTURE OF PILLARHALL CHIP

Schematically, a section of the studied PillarHall chip structure is shown in Fig. 1(a).[13,16,17] This chip with a size of $15 \times 15\,\mathrm{mm}^2$ is produced on a silicon wafer substrate with thickness around $400\,\mu$m. A polycrystalline silicon (PolySi) membrane on top of the structure with a nominal vertical thickness of 1500 nm is supported by $4\,\mu$m diameter pillars located at the distance of $50\,\mu m$ from each other.[16] An air gap with a nominal 500 nm height is formed between the PolySi membrane and the substrate. The PillarHall test chip includes several test structures with similar layers, described above, but different lateral sizes.[17] For reflectometry measurements, only the largest section with a size of about $5 \times 10\,\mathrm{mm}^2$ was used.

The PillarHall test chip is designed for evaluating the conformality of thin films during atomic layer deposition and chemical vapor deposition processes.[15–17] After the coating is applied, as shown in Fig. 1(b), the top membrane layer can be removed to assess the coating's uniformity and penetration depth.

PillarHall chip has complex periodic structural features related to the air gap. The microscope photograph of the PillarHall chip in Fig. 2 shows that the PolySi membrane has small and big dots on its surface. Big dots are related to pillars, but small dots are dips on the surface of the membrane, caused by the manufacturing process. The distance between the dips is approximately $7\,\mu$m, and their diameter is around $2\,\mu$m. Schematically, these structural features are shown in Fig. 1 as well.

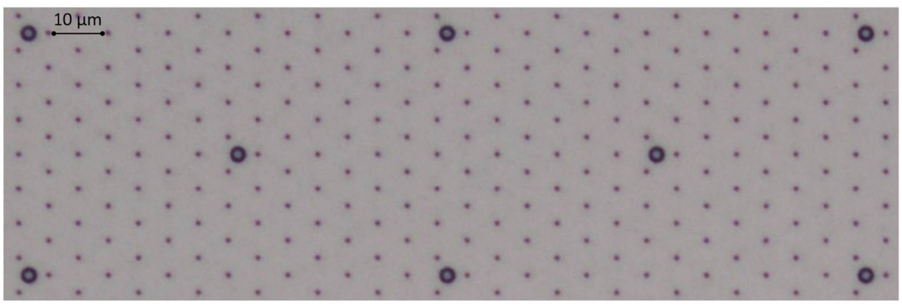

FIG. 2. Microscope photograph of PillarHall chip. Big dots are related to pillars. Small dots are dips on the surface of the membrane.

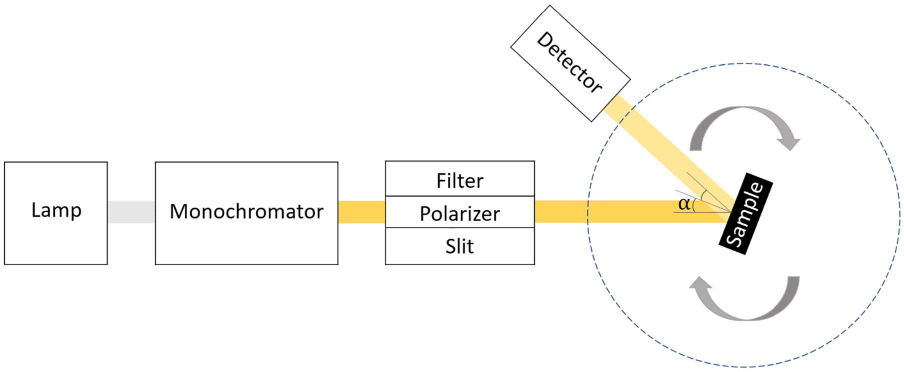

FIG. 3. Schematic presentation of the measurement setup.

III. MEASUREMENT SETUP

Reflectometry measurements of PillarHall samples, shown schematically in Fig. 3 were carried out using Cary 7000 spectrometer.[18] The incidence angle of the polarized light beam is $\alpha = 11°$ from normal with transverse dimensions of $3 \times 3\,mm^2$. The reflected light is collected to sandwich the Si/InGaAs detector with a focusing mirror of $40 \times 20\,mm^2$. The monochromator scans the wavelength over the range of 550–1800 nm. The bandwidth of the monochromator was 2 nm over the whole wavelength range. The raw measurement data were processed with the Richardson–Lucy (RL) bandwidth correction method[19] so that the final wavelength range used for the analysis is 560–1790 nm. All measurement settings and parameters are presented in Table I.

PillarHall chip has a structure with lateral periodicity; therefore, it may be that the incident light produces diffraction peaks. Angular scans were performed, when the incidence light angle was fixed to 11° while the detector viewing angle was changed over a wide range of 0°–40° relative to the normal of the sample surface. These measurements did not reveal any significant diffraction peaks exceeding 0.1% relative to the reflected intensity within the wavelength range from 560 to 1790 nm.

TABLE I. Settings and parameters of the measurement setup.

Measurement parameter name	Status
Light beam incidence angle α	11°
Light beam size on the sample	$3 \times 3\,mm^2$
Light beam position on the sample	Fixed
Polarization	Unpolarized (average of s- and p-polarizations)
Bandwidth	2 nm
Measured wavelength range	550–1800 nm
Wavelength range used (after applying RL method)	560–1790 nm
Detecting area	$40 \times 20\,mm^2$
Distance between the sample and detecting area	160 mm

IV. ANALYSIS OF REFLECTOMETRY DATA

A. Input data and fitting software

A single bandwidth-corrected reflectance spectrum of the PillarHall sample from 560 to 1790 nm is used as the input data. For the data analysis, a dedicated MATLAB code is used, which utilizes the transfer matrix method (TMM)[13] for calculating the reflectance from the layer structure of the sample and fits this modeled spectrum to the measured spectrum. The layer-structure model of the sample requires the thickness of each layer and values of the real (n) and imaginary (k) parts of the refractive index at each wavelength for each layer. The software tries to find the optimal thickness within the given range of possible values. In the same way, it is also possible to fit refractive indices, if they are described by equations, where coefficients are used as the fitted parameters.

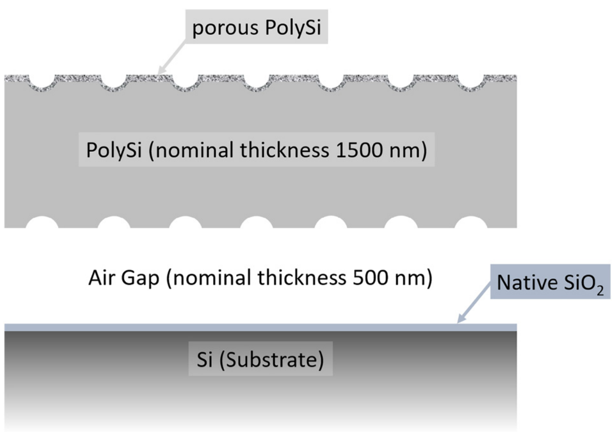

FIG. 4. Four-layer PillarHall model with nominal thickness values. The model takes into account the PolySi thickness variation, which is in reality caused by structural dips; however, in the model, it is not specified as dips but as the width of the thickness distribution. The dips have a diameter of around 2000 nm and a distance of 7000 nm between them. Only one fixed thickness of the native SiO_2 layer is included in the model.

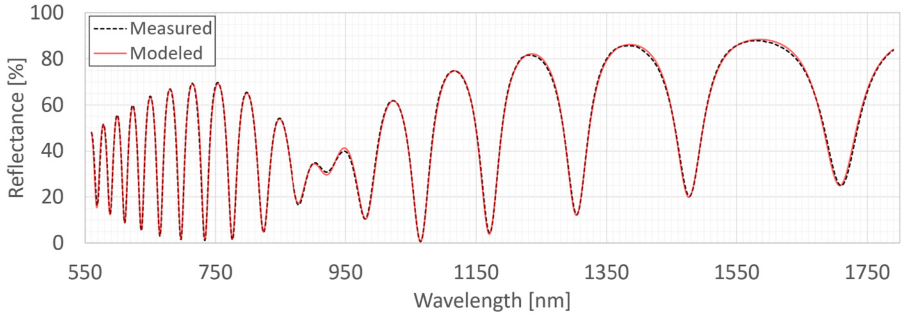

FIG. 5. Measured reflectance data and fitting results for the four-layer PillarHall model of Fig. 4. Root mean squared error between the model and measurement is 0.92%.

B. Basic model for the analysis

The analysis of reflectometry measurement data of the PillarHall sample with a nominal 500 nm air gap begins with a four-layer model, as depicted in Fig. 4. The parameters in this model include the thicknesses of the native SiO_2[20] on the silicon substrate, the air gap, and the PolySi layer; the width of the PolySi thickness distribution; and the complex refractive index of the PolySi layer, described using simplified Sellmeier equations.[21] Refractive indices of air and the silicon substrate[22] are kept fixed.

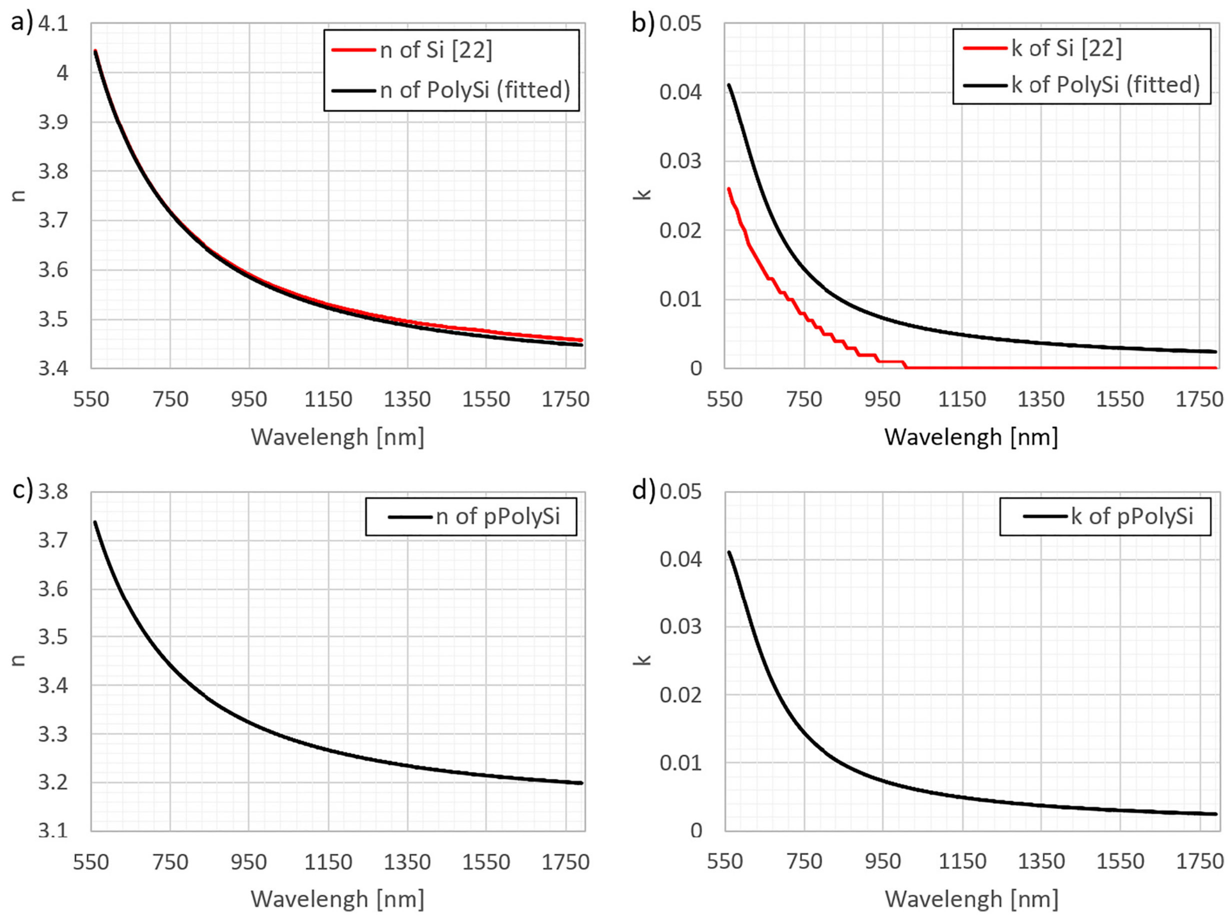

FIG. 6. Fitted real (n) and imaginary (k) parts of the refractive index of PolySi for the four-layer model, compared to the refractive index of silicon [(a) and (b)]. Fitted real (n) and imaginary (k) parts of the effective refractive index of pPolySi [(c) and (d)].

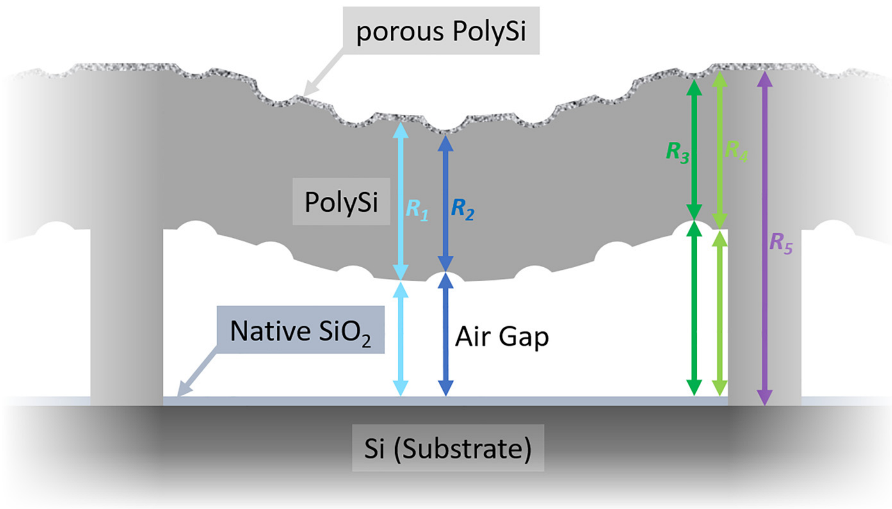

Reflectance case	Air Gap	PolySi
R_1	D_{AG}	D_{PolySi}
R_2	$D_{AG}+\Delta D_{PolySi}$	$D_{PolySi}-2\Delta D_{PolySi}$
R_3	$D_{AG}+\Delta D_{AG}+\Delta D_{PolySi}$	$D_{PolySi}-2\Delta D_{PolySi}$
R_4	$D_{AG}+\Delta D_{AG}$	D_{PolySi}
R_5	-	$D_{AG}+\Delta D_{AG}+D_{PolySi}$

FIG. 7. Advanced four-layer PillarHall model with five reflectance cases and corresponding thicknesses of layers displayed (schematic side view).

Polycrystalline silicon consists of crystals of varying sizes arranged in random orientations. The PolySi layer may contain small cavities, especially near the surface. An earlier analysis indicates that the description of the PolySi layer needs to include another layer close to the uppermost surface due to the short penetration depth of light in PolySi at around 600 nm wavelengths.[13] To account for the measured reflectance at these short wavelengths, an additional layer of porous polycrystalline silicon (pPolySi) is added to the model as shown in Fig. 4. The effective refractive index of this layer depends on the volume of the voids (air) in a host material (PolySi), which is described by the Bruggeman effective medium approximation.[23,24]

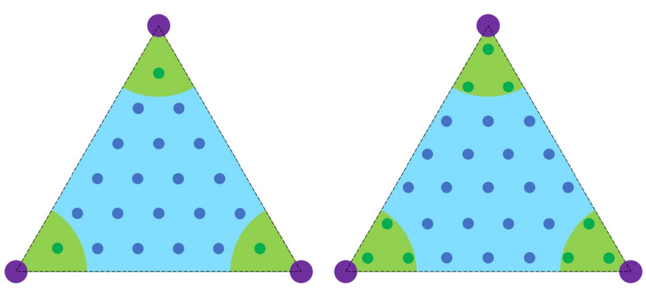

FIG. 8. Schematic presentation of the contribution of each reflectance case in two configurations of the triangular structural unit of the PillarHall chip (top view) with 21 (left) and 28 dips (right).

Each fitted parameter has its signature effect on the reflectance spectrum, as shown in Fig. 5. The thickness of the air gap layer affects the position of the envelope curve of the dense oscillations. The PolySi thickness changes the number and phase of the dense oscillations. The pPolySi layer influences the average reflectance up to approximately 700 nm wavelength.

PillarHall structural features, earlier mentioned as dips, lead to a thickness variation in the membrane. Therefore, it is unlikely that the thickness of the PolySi layer is uniform within the measurement beam spot. To account for PolySi thickness variations, the fitting of the four-layer model uses a narrow uniform distribution of thickness values of the PolySi layer around the fitted average value. The width of the thickness distribution affects the amplitude of the oscillations, especially at short wavelengths of the reflectance spectrum.

The fitted reflectance spectrum of the four-layer model, shown in Fig. 5, revealed that the air gap thickness is 464 nm and the PolySi layer thickness values are between 1460 and 1468 nm within the beam size, where the difference of 8 nm comes from the width of the thickness distribution. The fitted thickness of

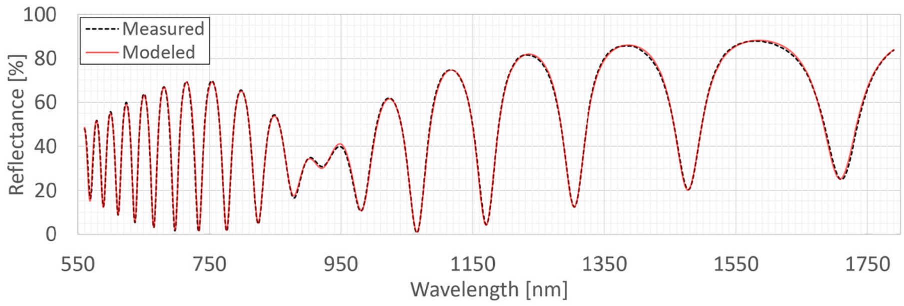

FIG. 9. Measured reflectance data and fitting results for the advanced four-layer PillarHall model of Fig. 7. Root mean squared error between the model and measurement is 0.88%.

the pPolySi layer, which is on the top of the PolySi layer, is 24 nm with the volume fraction of air of 11%. The fitted thickness value for the pPolySi layer at the bottom of the PolySi layer (between PolySi and air gap) is close to zero—this is why this layer is not shown in Fig. 4. The native SiO_2 layer on top of the Si substrate has a fixed thickness of 3 nm. The fitted curves for the refractive index (n) and extinction coefficient (k) of both pPolySi and PolySi, compared to silicon, are displayed in Fig. 6. If there would be some loss of reflected intensity due to diffraction as described in Sec. III, it would only cause an apparent increase in the imaginary part of the PolySi layer refractive index in Fig. 6(b).

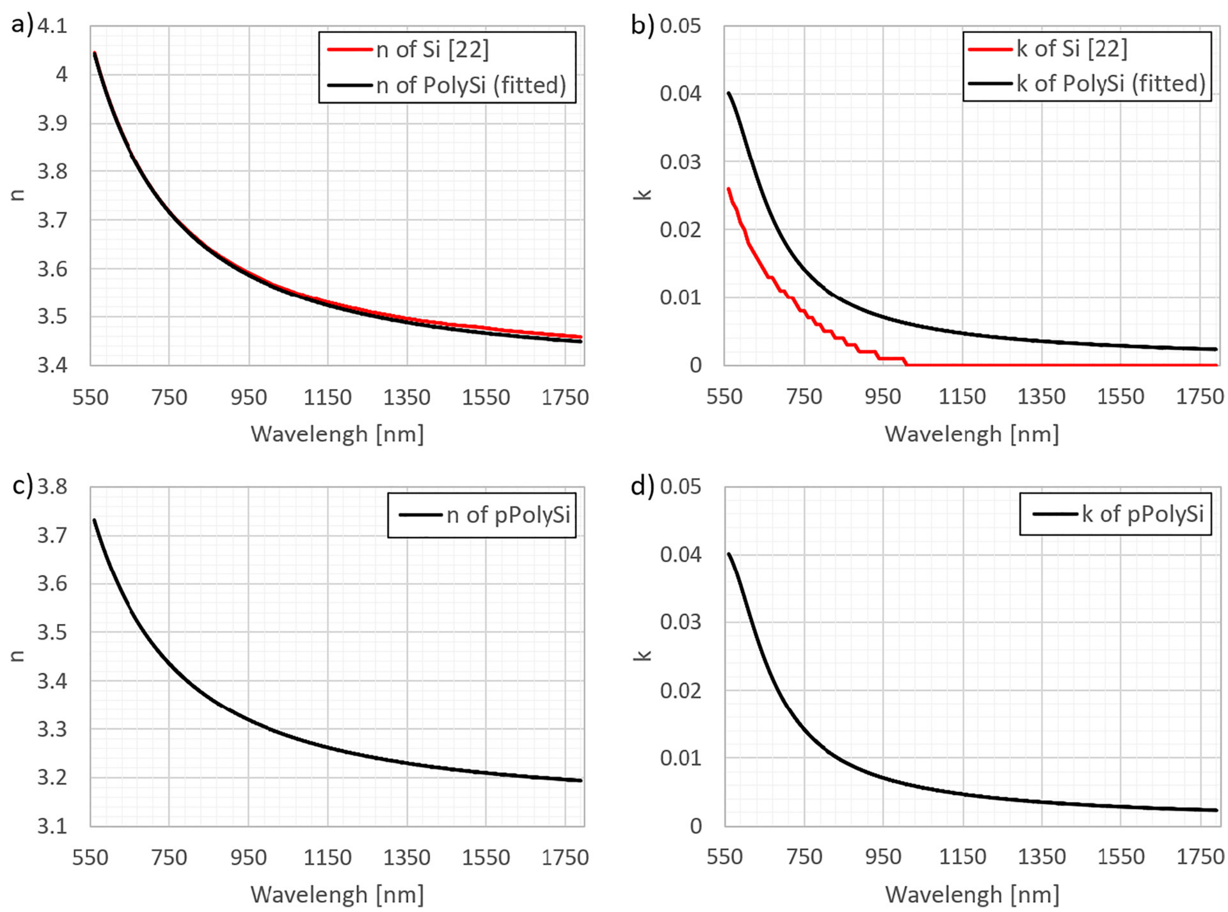

FIG. 10. Fitted real (n) and imaginary (k) parts of the refractive index of PolySi for the advanced four-layer model, compared to the refractive index of silicon [(a) and (b)]. Fitted real (n) and imaginary (k) parts of the effective refractive index of pPolySi [(c) and (d)].

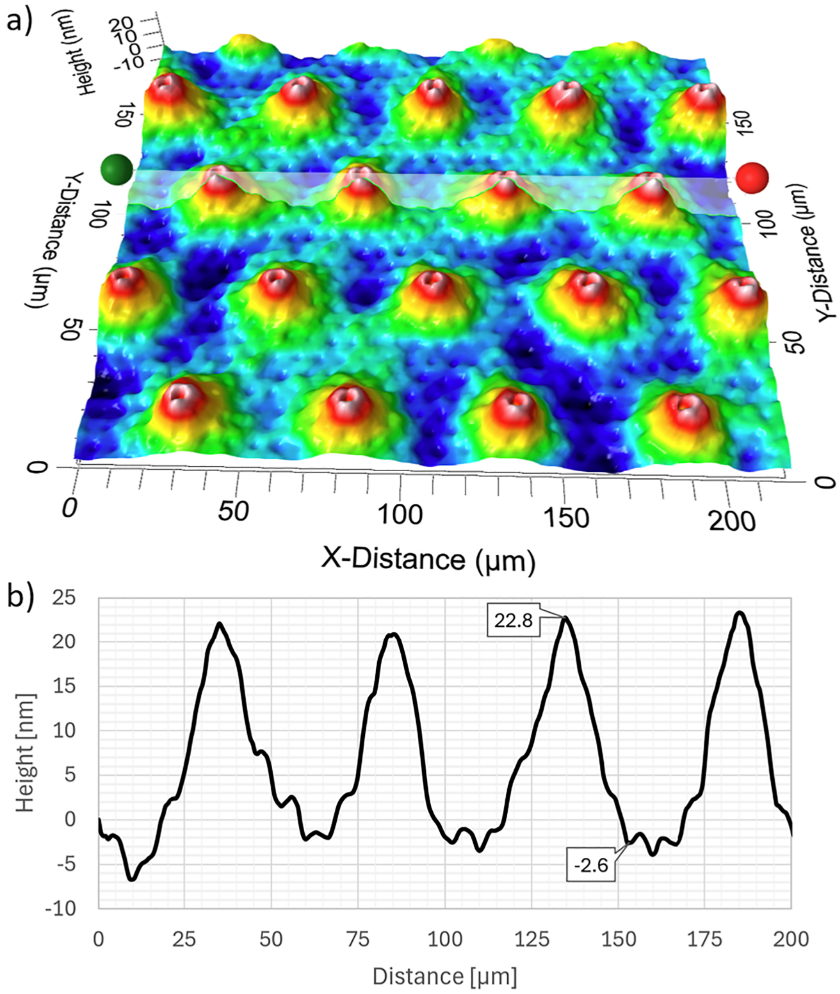

FIG. 11. (a) Bending amplitude between pillars of the PillarHall sample observed through optical profilometer imaging. (b) Green and red balls indicate the location of the cross section of the profile scan.

C. Advanced model for the analysis

The four-layer model, which is described above, has the width of PolySi thickness distribution as a fitted parameter. To enhance the model, also the width of air gap thickness distribution may be included in the model. However, combining both PolySi and air gap thickness distribution parameters is not that straightforward since there might be many combinations possible. Excluding all unnecessary combinations requires a closer look at the PillarHall membrane structure.

In the case of the PolySi membrane, the thickness variation is caused by dips on the PolySi surfaces. For the air gap thickness, the variation is conditioned by the same membrane dips but also by membrane bend between pillars. Therefore, the PillarHall structure is laterally periodic, and it is possible to find certain combinations of PolySi and air gap thickness variations, describe them mathematically, and put them into the reflectance model.

Considered reflectance cases are presented schematically in Fig. 7, where each arrow color corresponds to a certain reflectance case with a unique combination of PolySi and air gap thicknesses. Five cases are associated with the air gap (AG), where there is air gap thickness D_{AG} in the middle between pillars and thickness $D_{AG} + \Delta D_{AG}$ near the pillars. Parameter ΔD_{AG} describes the average bending of the PolySi membrane. Furthermore, because of dips in the membrane, we have an additional variation component ΔD_{PolySi}. The fifth case is associated with reflectance from pillars.

To calculate the reflectance with the layer model of Fig. 7, it is necessary to estimate the relative contribution of each case. Figure 8 shows two configurations of the area limited by three pillars with 21 or 28 dips inside. The equilateral triangular area represents the basic structural unit of the PillarHall sample. By calculating area ratios within these triangles and then averaging them, it is possible to approximately estimate the contribution of each reflectance case to the total reflectance. In Fig. 8, each area color represents the corresponding reflectance case as shown in Fig. 7. The analysis of the PillarHall chip photograph, shown in Fig. 4, and the knowledge that the pillar diameter is $4\,\mu$m and the distance between pillars is $50\,\mu$m,[16] allows us to estimate that the diameter of the dips is $2\,\mu$m and the distance between them is $7\,\mu$m. Based

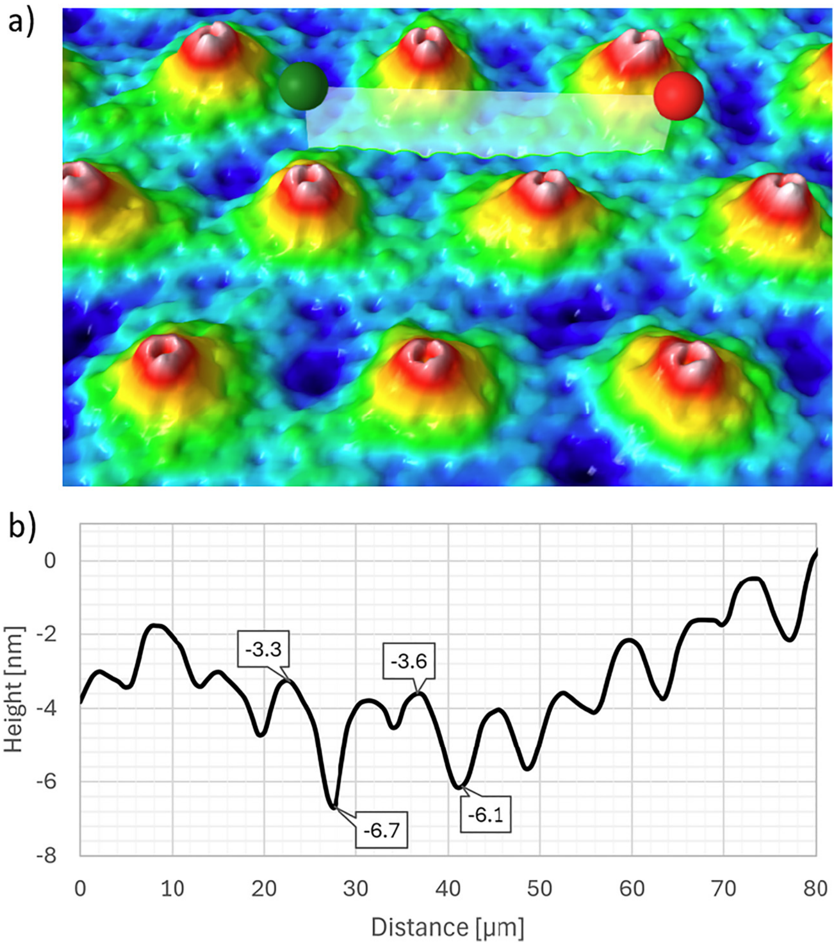

FIG. 12. (a) Height of the dips observed through optical profilometer imaging. (b) Green and red balls indicate the location of the cross section of the profile scan.

on this information, the relative contribution of the reflectance of the pillars (R_5) is 0.6% (marked with purple color). The average reflectance of the area near the pillars (R_4), with the radius of one quarter of the pillar distance, has the relative contribution of 18.6% (light green color) and the average reflectance of the dips (R_3) near the pillars has the relative contribution of 1.7% (dark green color). The remaining dips (R_2) reflect 5.4% of the light (dark blue), and the area around them (R_1) gives the rest of the total reflectance (light blue). Each of these reflectance cases is described in the fitting software by appropriate layer structure, and then, the total reflectance is calculated as the weighted average, as shown in Fig. 8.

The fitted reflectance spectrum of the advanced four-layer model, shown in Fig. 9, reveals that the air gap thickness parameter varies between $D_{AG} = 460$ nm and $D_{AG} + \Delta D_{AG} = 475$ nm (without dips). An important note here is that $D_{AG} + \Delta D_{AG}$ is not the air gap height right next to the pillar, but the average thickness in the area around the pillar with the radius of 12 μm corresponding to R_4 reflectance, which occupies 18.6% of the area of the chip. The same is true for other fitted parameters, where the fitting gives an average value within the colored area shown in Fig. 8. The average PolySi layer thickness within the beam size varies between D_{PolySi}−$2\Delta D_{PolySi} = 1455$ nm and $D_{PolySi} = 1464$ nm with dips $\Delta D_{PolySi} = 5$ nm in depth. The pPolySi layer thickness is $D_{pPolySi} = 23$ nm with the volume fraction of air of 11%. The SiO_2 interface layer has the same fixed thickness of 3 nm as in the basic model. The fitted curves for the refractive index (n) and extinction coefficient (k) of both pPolySi and PolySi, compared to silicon, are displayed in Fig. 10.

Sensitivity tests were made on the reflectance component weights of the equation in Fig. 8. A change in the dip diameter from 2 μm to 3 μm indicated a reduction in the fitted dip height less than 2 nm. Similar sensitivity tests on other reflectance component weights resulted in even smaller variations of the fitted parameters.

An estimate of the actual bending amplitude of the PolySi membrane can be made with the help of the fitted result $\Delta D_{AG} = 15$ nm by assuming that the cross sections of the bent surfaces can be described by upward bending (light blue area in Fig. 8) and downward bending (light green area in Fig. 8) parabolic curves. Then, the cross section is revolved around the pillar and the average change in the air gap height in the light blue and light green areas is calculated. The fraction of 12% of the light blue area,

TABLE II. PillarHall parameters obtained with reflectometry (basic model and advanced model) and profilometry. The thickness ranges of advanced model are obtained using equations in Fig. 7.

Reflectometry and basic model	Air gap height		Average PolySi thickness	Width of PolySi thickness distribution	pPolySi thickness	Air % in pPolySi
			1464 nm ± 5 nm	8 nm ± 8 nm		
	464 nm ± 2 nm		PolySi thickness range 1460–1468 nm		24 nm ± 5 nm	11%
Reflectometry and advanced model	Air gap height (without dips) D_{AG}	PolySi bending[a] $1.5\Delta D_{AG}$	PolySi thickness D_{PolySi}	PolySi dip height ΔD_{PolySi}	pPolySi thickness	Air % in pPolySi
	460 nm ± 6 nm	23 nm ± 23 nm	1464 nm ± 8 nm	5 nm ± 5 nm		
	Air gap thickness range[a] 456–479 nm		PolySi thickness range 1455–1464 nm		23 nm ± 5 nm	11%
Profilometry	Air gap height	PolySi bending	PolySi thickness	PolySi dip height	pPolySi thickness	Air % in pPolySi
	…	25 nm	…	3 nm	…	…

[a]Values calculated from the average PolySi membrane bending of $\Delta D_{AG} = 15$ nm within the given areas using a parabolic bending model.

which is not covered by the revolved surfaces, is assumed to have a constant air gap. This calculation gives the result that the peak-to-peak variation in the air gap height is $1.5\Delta D_{AG} = 23$ nm.

D. Comparison between methods

To validate the results determined from reflectometry, an optical profilometer (Bruker, ContourX-500) was also used for the characterization of the PillarHall sample surface. The sample was analyzed in the phase-shifting interferometry mode. As presented in Figs. 11 and 12, the bending amplitude around pillars is approximately 25 nm, and the height of dips is approximately 3 nm.

Comparison of the results obtained with the basic model, the advanced model and surface scanning using profilometer are shown in Table II. It shows capabilities of the models and methods describing how their results correspond to each other. The average air gap and PolySi thicknesses determined by the basic and advanced reflectance models are in good agreement, although the advanced model transfers 4 nm of thickness from PolySi to the air gap, as determined from the centers of the quoted thickness ranges. Bending of the PolySi membrane can be determined from reflectometry results only when using the advanced model for analysis. The width of the PolySi thickness distribution of the basic model can be affected also by the large scale thickness variation of the membrane. Parameters describing the porous PolySi layer are in very good agreement when determined by either the basic or advanced model.

While comparing the profilometry and reflectometry results, it is worth mentioning that the average bending height within the corresponding reflectance areas cannot be directly compared with profilometry results, since the profilometer shows the actual membrane bending. With this background, the agreement reached in PolySi bending from profilometry and reflectometry, with parabolic description of bent surfaces, is remarkably good. Good agreement is also achieved in PolySi dip heights, although both methods are close to their performance limit with these feature sizes of a few nanometers. A significant advantage of the reflectometry methods is that they can give information on the air gap and PolySi layer thicknesses, parameters that are inaccessible with profilometry.

The results of basic and advanced models are accompanied by uncertainty estimates, as shown in Table II. In the uncertainty estimation method, the target parameter (e.g., a specific layer thickness) is manually adjusted within a defined range while other parameters are kept free for fitting. The algorithm compensates for changes in the adjusted target parameter by optimizing the remaining parameters. When the weakening in fitting quality becomes visually noticeable, the difference between the adjusted target parameter value and its optimal value is taken as the uncertainty estimate. Due to the inherent limitations of the reflectometry method, particularly for features on the scale of a few nanometers, the fitting software exhibits low sensitivity to such small variations, resulting in high relative uncertainty estimates for these features.

V. CONCLUSIONS

This work demonstrates the applicability of reflectometry methods to the characterization of complex periodic multilayer thin-film structures, such as the studied PillarHall sample, using a single large-beam measurement. Both considered models, basic and advanced, provide a good fit between the measurements and simulated spectra with a root mean squared error between the model and measurement of around 0.9%. The basic model is sufficient for general structural characterization, yielding accurate layer thicknesses, including a 464 nm air gap and the method even shows the range of thicknesses of 1460–1468 nm for the PolySi layer. The advanced model's ability to incorporate structural complexities provides an improved understanding of PillarHall chips, introduces a more detailed analysis, and identifies the air gap thickness range of 456–479 nm and PolySi thickness range of 1455–1464 nm across the chip surface. The advanced model also gives information on the size of PillarHall structural features, such as air gap bending of 23 nm and 5 nm dips depth of the PolySi membrane. The reflectometry results are close to those parameter values, which can be determined by profilometry, especially when describing the PolySi layer bending by a parabolic shape.

Thus, the basic model is suitable when no prior information about the sample's structural features is available. The advanced model has an advantage when the sample's structural features are known, but their precise longitudinal dimensions remain undefined.

ACKNOWLEDGMENTS

The project 20IND04 ATMOC leading to this publication has received funding from the EMPIR program co-financed by the participating states and the European Union's Horizon 2020 research and innovation program, Funder ID: 10.13039/100014132. The work is part of the Research Council of Finland Flagship Programme, Photonics Research and Innovation (PREIN), Decision No. 346529, Aalto University.

AUTHOR DECLARATIONS

Conflict of Interest

The authors have no conflicts to disclose.

Author Contributions

Aleksandr Danilenko: Investigation (equal); Software (equal); Visualization (equal); Writing – original draft (lead). **Masoud Rastgou:** Investigation (equal); Writing – review & editing (equal). **Farshid Manoocheri:** Investigation (equal); Writing – review & editing (supporting). **Jussi Kinnunen:** Investigation (equal); Resources (equal); Writing – review & editing (equal). **Virpi Korpelainen:** Investigation (equal); Resources (equal); Writing – review & editing (equal). **Antti Lassila:** Resources (equal); Writing – review & editing (supporting). **Erkki Ikonen:** Investigation (equal); Supervision (lead); Writing – review & editing (equal).

DATA AVAILABILITY

The data that support the findings of this study are available from the corresponding author upon reasonable request.

REFERENCES

[1]J. K. Lee, S. Y. Park, Y. H. Kim, J. C. Lee, J. H. Lee, C. H. Lee, and Y. H. Sung, in *Proceedings of the IEEE 69th Electronic Components and Technology Conference (ECTC)* (IEEE, 2019), pp. 35–40.

[2]Y. J. Mii, in *Proceedings of the IEEE Symposium on VLSI Technology and Circuits* (IEEE, 2022), pp. 276–281.

[3]S. Zhang, Z. Li, H. Zhou, R. Li, S. Wang, K. W. Paik, and P. He, e-Prime Adv. Electr. Eng. Electron. Energy **2**, 100052 (2022).

[4]H. Bender, O. Richard, A. Kalio, and E. Sourty, Microelectron. Eng. **84**(11), 2707–2713 (2007).

[5]M. Urbánek, J. Spousta, T. Běhounek, and T. Šikola, Appl. Opt. **46**(25), 6309–6313 (2007).

[6]B. Fu and M. A. Gribelyuk, J. Appl. Phys. **123**(16), 161554 (2018).

[7]V. N. Sekhar, S. Neo, L. H. Yu, A. D. Trigg, and C. C. Kuo, in *Proceedings of the 12th Electronics Packaging Technology Conference* (IEEE, 2010), pp. 462–466.

[8]V. M. Bjelland, N. Hale, N. Schwarz, D. Vala, J. Høvik, and M. Kildemo, Opt. Express **32**(1), 703–721 (2024).

[9]M. Tanksalvala, C. L. Porter, Y. Esashi, B. Wang, N. W. Jenkins, Z. Zhang, G. P. Miley, J. L. Knobloch, B. McBennett, N. Horiguchi, S. Yazdi, J. Zhou, M. N. Jacobs, C. S. Bevis, R. M. Karl, P. Johnsen, D. Ren, L. Waller, D. E. Adams, S. L. Cousin, C.-T. Liao, J. Miao, M. Gerrity, H. C. Kapteyn, and M. M. Murnane, Sci. Adv. **7**(5), eabd9667 (2021).

[10]A. Haapalinna, F. Manoochehri, and E. Ikonen, Anal. Chim. Acta **380**(2–3), 317–325 (1999).

[11]S. Pourjamal, H. Mäntynen, P. Jaanson, D. M. Rosu, A. Hertwig, F. Manoocheri, and E. Ikonen, Metrologia **51**(6), S302 (2014).

[12]S. Danylyuk, S. Herbert, P. Loosen, R. Lebert, A. Schäfer, J. Schubert, M. Tryus, and L. Juschkin, Phys. Status Solidi C **12**(3), 318–322 (2015).

[13]A. Danilenko, M. Rastgou, F. Manoocheri, J. Kinnunen, V. Korpelainen, A. Lassila, and E. Ikonen, Meas. Sci. Technol. **34**(9), 094006 (2023).

[14]S. A. Furman and A. V. Tikhonravov, *Basics of Optics of Multilayer Systems* (Atlantica Séguier Frontieres, 1992).

[15]K. Arts, M. Utriainen, R. L. Puurunen, W. M. M. Kessels, and H. C. M. Knoops, J. Phys. Chem. C **123**(44), 27030–27035 (2019).

[16]J. Yim, O. M. E. Ylivaara, M. Ylilammi, V. Korpelainen, E. Haimi, E. Verkama, M. Utriainen, and R. L. Puurunen, Phys. Chem. Chem. Phys. **22**, 23107–23120 (2020).

[17]M. Utriainen, K. Saastamoinen, H. Rekola, O. M. E. Ylivaara, R. L. Puurunen, and P. Hyttinen, Proc. SPIE **12008**, 120080D (2022).

[18]Agilent Technologies, *Agilent Cary Universal Measurement Accessory (UMA)* (2013).

[19]A. Danilenko, M. Rastgou, F. Manoocheri, and E. Ikonen "Application of a bandwidth correction method to thin-film reflectance measurements" (unpublished).

[20]I. H. Malitson, J. Opt. Soc. Am. **55**(10), 1205–1209 (1965).

[21]J. A. Dobrowolski, F. C. Ho, and A. Waldorf, Appl. Opt. **22**(20), 3191–3200 (1983).

[22]M. A. Green, Sol. Energy Mater. Sol. Cells **92**(11), 1305–1310 (2008).

[23]G. Bruggeman, Ann. Phys. **416**(7), 636–664 (1935).

[24]M. Sela and C. Haspel, Appl. Opt. **59**(28), 8822–8827 (2020).